Advances in Science and Technology Research Journal

*Advances in Science and Technology Research Journal*, 18(7), 62–77
https://doi.org/10.12913/22998624/192638
ISSN 2299-8624, License CC-BY 4.0

Received: 2024.07.04
Accepted: 2024.09.18
Published: 2024.10.06

# The Influence of Impact Velocity on Stresses and Failure of S355J2 Steel Under Slurry Erosion Conditions

Marta Halina Buszko[1*], Dominika Ewa Zakrzewska[2]

[1] Department of Erosion Processes, Centre of Hydrodynamics, The Szewalski Institute of Fluid-Flow Machinery, Polish Academy of Sciences, ul. Fiszera 14, 80-231 Gdansk, Poland

[2] Department of Manufacturing and Production Engineering, Faculty of Mechanical Engineering and Ship Technology, Gdansk University of Technology, ul. Narutowicza 11/12, 80-233 Gdansk, Poland

* Corresponding author's e-mail: marta.buszko@imp.gda.pl

## ABSTRACT

The purpose of this work was to determine the essence of the influence of the impact velocity (5, 7, and 9 m/s) on Hertzian stresses and the erosion mechanism of ferritic-pearlitic S355J2 steel. The investigations were carried out using a slurry pot tester. S355J2 steel showed a strong sensitivity to changes in impact velocity. A significant increase in erosion rate was observed at a velocity of 9 m/s. This increase was 5-fold and over 15-fold compared to velocities of 7 m/s and 5 m/s, respectively. The study of Hertzian stress is crucial in erosion research because it helps understand how impact energy is absorbed by the eroded material and the mechanisms that cause surface wear. A linear increase in mean contact pressure and maximum shear stress was observed with increasing impact velocity. The mean contact pressure increased from 4.3 GPa to 5.5 GPa and the maximum shear stress increased from 2.0 GPa to 2.5 GPa. The kinetic energy of the solid particles that hits the eroded steel is distributed in the contact area, which leads to various deformations and wear mechanisms. The primary type of deformation was fatigue degradation of the surface layers of the eroded steel. The high kinetic energy of solid particles contributed to the formation of plastic deformations and strongly deformed steel flakes. Higher impact velocities generally result in greater forces and contact stresses on the material surface. This led to the intensification of plastic deformation in the contact areas and increased the Hertzian stresses.

**Keywords:** slurry erosion, steel, Hertzian stresses, hardness, degradation mechanism.

## INTRODUCTION

Slurry erosion occurs when solid particles suspended in a liquid medium impact the eroded surface with sufficient force (energy) to cause damage and loss of material [1, 2]. Slurry erosion take places in various industrial sectors. This type of erosion is often seen in the oil, gas and mining industries. These sectors mainly use carbon steel pipes, which provide a cost-effective and versatile method of delivering these resources from extraction sites to users [3–6]. During slurry erosion numerous parameters interact simultaneously, resulting in a synergistic effect. Factors influencing slurry erosion are multifaceted and include operating conditions (such as impact velocity, impingement angle, and solid particle concentration), properties of the eroding particles (including shape, size, and hardness), and characteristics of the target material (such as microstructure, hardness, ductility, as well as yield and ultimate strengths) [1, 3, 7, 8]. This type of erosion is similar to the shot peening process, where round solid particles (balls) are used due to their ability to distribute stress evenly in the surface layer of the material, resulting in better mechanical properties, such as fatigue strength. Although slurry erosion and shot peening have different objectives, both processes are based on the interaction of the material surface with particles and lead to structural changes of the surface [9–11]. Impact velocity is a critical factor in slurry erosion, directly

affecting the kinetic energy of the solid particles and the resulting stresses generated in the eroded material. Many researchers have studied the impact of solid particles velocity on erosion rate [12–16]. The velocity of the erodents exhibits an empirical power-law relationship with erosion rate [17–19]:

$$ER \sim kV^n \quad (1)$$

where: $ER$ represents the erosion rate, $V$ is the impact velocity of solid particles (erodents), $k$ is a constant and $n$ is the impact velocity exponent, which ranges from 0.34 to 4.83 and depends on operational conditions, target material properties, and erodents [1, 20–22].

This relationship highlights the power effect of impact velocity on erosion, emphasizing the importance of controlling operating conditions to minimize the wear of materials.

Higher impact velocities generate higher kinetic energy of solid particles and thus lead to more serious interactions with the eroded surface of the tested material [12, 23, 24]. As with impact velocity, the size of the solid particle also plays an important role. An increase in the size of the solid particles at a constant concentration reduces the number of particles in the medium, while also increasing the kinetic energy of the impact of the solid particles on the eroded surface [25–28]. Ultimately, this leads to increased stresses, which may cause plastic deformation, fatigue of the surface of the eroded material, and even brittle fracture [17]. Krella et al. [6] carrying out slurry erosion tests on X10CrAlSi18 ferritic steel using cast steel round solid particles (520 μm), it was observed that the importance of craters in the erosion process decreased with the increase in the impact velocity, but erosion rate increased. It was connected with a platelet mechanism (steel flakes) that occurred at higher velocities. Desale et al. [25] showed that the increase in erosion rate was due to the increase in the size of the erodents (quartz particles) in slurry suspension from 37.5 um to 655 um. At the impact angle of 90º, no significant differences in the erosion mechanism were observed with respect to the size of the quartz particles, mainly deformational wear was visible. In general, solid particles with sharp and irregular edges lead to increased erosion rates than rounded solid particles because they create deeper indentations, pits and craters with irregular edges [29, 30]. Vite-Torres et al. [31, 32] testing two different steels (AISI D2 and AISI 420) under the same erosion conditions using steel round grit particles and angular silicon carbide (SiC). The erodents size was in the range of 400–420 μm. The tests conducted in the air jet rig showed that the erosion rate caused by spherical particles was twice as low as compared to irregular SiC particles, regardless of the impact angle. After erosion tests using round steel solid particles, the eroded surfaces showed pitting, scratches, craters, debris, and steel flakes. The type of material of the solid particles and therefore its hardness or density, as well as their shape and size described above, is a factor that significantly affects the erosion rate. In general, solid particles that are harder than the material being eroded lead to an increased erosion rate [15, 33]. Moreover, when a solid particle collides with the material being eroded, they can fragment and crack, or round off in the case of sharp-edged particles [24, 34]. Higher-density particles have more mass for the same volume. At a given impact velocity, their kinetic energy is greater than lower-density solid particles. According to the research on the shot peening process conducted by Świetlicki et al. [35], the type of material had a significant influence on the material's deep hardening. The impact of the balls (ceramic, glass and steel) on the tested surface of additive-manufactured 17-4PH steel increased hardness in the material's deepest parts due to compressive residual stresses. The depth of these stresses depends on the energy of a single ball, which is influenced by its mass at constant peening pressure. The hardening depth was 40, 60, and 80 μm using ceramic particles, glass beads and steel shot, respectively

Regardless of the medium in which the tests are carried out, the same dependences were obtained regarding the impact velocity or properties of erodents. Nevertheless, the medium in which the erosion process takes place has a significant influence on the erosion mechanisms and the rate of material wear. Air, as a low-density medium, allows for higher particle velocities, which can lead to intensive surface erosion. Water, due to its higher density and viscosity, causes slower movement of particles, but a greater impact force can lead to significant damage [14, 36].

In order to reduce the erosion of structural steel, various coatings are deposited. Typically these are cermets [37, 38].

According to Hertzian contact mechanics, a particle impinging on the surface of tested

material will create localized stresses (normal and tangential) that may cause plastic deformation and, therefore, material removal [39, 40]. Johnson [40] emphasized that the contact stresses in the Hertzian contact increase with the increase in the impact velocity, which is the result of the increase in kinetic energy converted into mechanical stresses. In [41] it was also found that as the velocity increases, higher stresses occur in the tested material and the damage penetration increases. In general, the response of steel to such stresses depends on its microstructure and mechanical properties. Steel can be subject to significant work hardening due to high-velocity impacts, which would change the surface hardness and even further improve resistance up to some limit [42]. However, continuous high-velocity impacts may also lead to the initiation and propagation of microcracks, surface spalling, and increased material loss, leading to a decreasing overall erosion resistance [4, 43]. Katsumata et al. [44] investigated the influence of the shape and size of solid particles on the erosion of TiN coating. Katsumata et al. [44] found that spherical particles with a 3 μm diameter induce plastic deformation and microcracking from fatigue, resulting in cracks on the surface and within the coating. The impact stresses were low since the striking area on the eroded surface was vast and the Hertzian stress caused maximum shear stresses to occur at a specific depth.

S355J2 steel grades are the structural low-carbon steel grades that are applied in many industries. It is often used for industrial pipes, pipelines supplying gas and oil, hulls of ships, structural elements, and welded structures [45–47]. Due to the wide use of these steel grades for components exposed to slurry, it is important to know how these steels degrade, the influence of impact velocity on the degradation process resistance and what their erosion resistance is. Although their strength properties are lower than those of higher-quality steels, their price-quality ratio is a great advantage.

Because S355J2 steel is popular in many applications, it is important to know its erosion resistance. Furthermore, the original environment used for slurry preparation, i.e., cast steel round solid particles, makes the slurry erosion similar to the shot peening process. In order to achieve this goal, the effect of impact velocity and exposure time on the erosion rates was investigated, as well as the effect of impact velocity on surface hardness and Hertzian stresses was analyzed. Understanding the effect of stresses, such as Hertzian stresses, on slurry erosion can help in designing more durable steel materials and systems. The degradation process was identified through surface analysis using scanning electron microscopy.

## MATERIALS AND METHODS

The tests were conducted using a rotary test rig (slurry pot), schematically depicted in Figure 1. This test rig primarily consists of a cylindrical tank with a 6.4-liter capacity, a mixing system, and a drive set. A propeller, attached to the end of the main drive shaft, ensures the prevention of sedimentation and the even distribution of solid particles (erodents) in the liquid medium. Four baffles are mounted on the walls of the slurry pot to disrupt the slurry flow and minimize fluid centrifugation. The samples are placed in two specimen holders, and the velocity is controlled with an inverter.

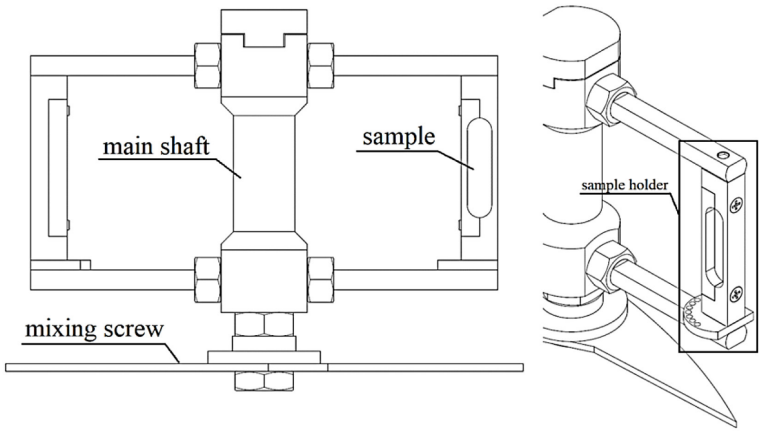


**Figure 1.** Slurry pot tester (scheme)

Erosion tests were performed on S355J2 low-carbon steel samples as delivered. S355J2 steel is characterized by a ferritic-pearlitic structure with fine grain (Figure 2a). Ferrite grains have a size of 7 ± 2 μm, while pearlite grains are 2 ± 1 μm. The pearlite content was about 21%. The samples had dimensions of 40 × 10 × 5 mm and the sample rounding radius was 5 mm. The hardness was 152 HV ± 4 HV, and the Young's Modulus was 210 GPa. Cast steel round solid particles (erodents) were used for erosion tests (Figure 2b). The erodents had a diameter of 0.52 ± 0.05 mm, a Vickers hardness of 528 HV, a Young's Modulus of 190 GPa and density of 7840 kg/m$^3$.

The tests were carried out for three impact velocities: 5 m/s, 7 m/s and 9 m/s. The angle of impact of solid particles on the eroded surface was 90º. The suspension consisting of solid particles and tap water had a concentration of 12.5%. Depending on the impact velocity used, the kinetic energy of a single solid particle was: 7.2 μJ (5 m/s), 14.1 μJ (7 m/s) and 23.4 μJ (9 m/s). However, taking into account the mass of all solid particles used in the erosion test, the kinetic energy was: 10.8 J (5 m/s), 21.1 J (7 m/s) and 34.8 J (9 m/s). The duration of the slurry erosion tests was 600 min (10 h).

The sample surfaces were ground and polished using diamond paste to obtain similar initial surface values. The samples prepared in this way were weighed on an XA160 analytical scale and measurements of hardness were performed on a INNOVATEST Falcon 401 Vickers hardness tester (300 gf load and dwell time of 10 s). Before and after each exposure to erosion damage, in order to determine the standard deviation, mass measurements were performed three times and hardness measurements four times. However, hardness tests on the cross-section of the tested steel were performed three times for each test condition (5, 7, and 9 m/s) after erosion tests. Observations of the eroded surface after erosion tests and on cross-sections were made on a Hitachi SU3500 scanning electron microscope (SEM), while microstructure studies were performed on a Neophot 2 optical microscope. 5% nital was used to obtain the microstructure. Grain size and pearlite content, size of solid particle, size of craters as well as the thickness of the deformed layer were determined using ImageJ software.

## RESULT AND DISCUSSION

### Slurry erosion tests

The conducted erosion tests in the form of erosion curves (Figure 3) provided a new insight

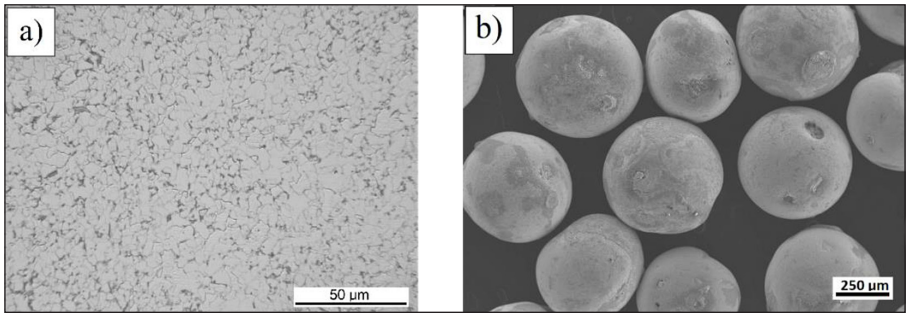


**Figure 2.** Microstructure of S355J2 steel (a) and cast steel solid particles (erodents) (b)

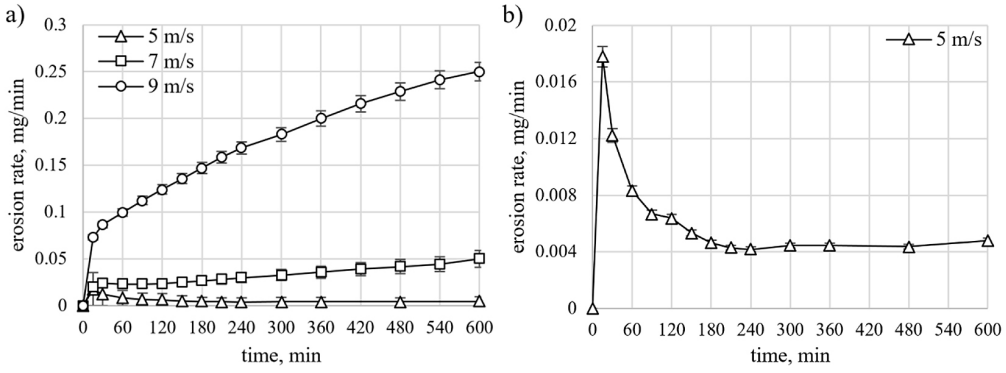


**Figure 3.** Erosion curves for (a) 5, 7 and 9 m/s, (b) 5 m/s

into the erosion of S355J2 low-carbon steel at three impact velocities (5, 7 and 9 m/s). A significant increase in erosion rate was observed at the highest impact velocity (9 m/s). This increase is fivefold and over fiftyfold compared to the velocity of 7 and 5 m/s, respectively.

In the case of the erosion curve obtained at velocity of 9 m/s, a constant increase in the erosion rate with exposure time was observed (Figure 3a). The tests carried out at 7 m/s show a different course of the erosion curve, although the maximum value occurs after 600 min of tests like at 9 m/s, the increase in the erosion rate is much slower (Figure 3a). Comparing the presented results with a velocity of 5 m/s, it was observed that after obtaining the maximum erosion rate value in 15 min of erosion test, erosion rate decrease until 240 min of test and then remain at a similar level until the end of the test (Figure 3a and b). In all cases, the largest increase in erosion rate occurred at the beginning of the erosion tests (first 15 min of testing). The increase in erosion rate with impact velocity is associated with the increase in kinetic energy of the erodents and the increase in impact frequency caused more effective damage on the steels surface. Moreover, such a large difference in erosion rate at the velocity of 9 m/s and different erosion curve profile (significant, continuous increase in erosion rate) indicate a change in the degradation process (increasing the intensity of erosion leads to faster removal of material from the surface, as well as higher stresses leading to the appearance of e.g. cracks).

The effect of impact velocity on erosion rate (Figure 4) is generally known [13, 15, 22]. It is described as also presented above using the Equation 1. In this case, a significant increase in the exponent *n* is visible (6.75), which is closely related to such a large increase in the erosion rate at 9 m/s and 7 m/s (Figure 3a). The higher the exponent *n*, the more susceptible the material is to the formation of cracks on the surface or below the surface (more aggressive erosion), which is consistent with SEM images (Figure 12). The increase in the hardness of the eroded material could also have contributed to the increase in the velocity exponent *n* [48]. Moreover, in [49] was shown that the highest values of the exponent *n* are obtained when the rotary test rigs are used. Such a test device was used in the present study (Figure 1). Thus, one of the reasons for the high exponents *n* was the test device.

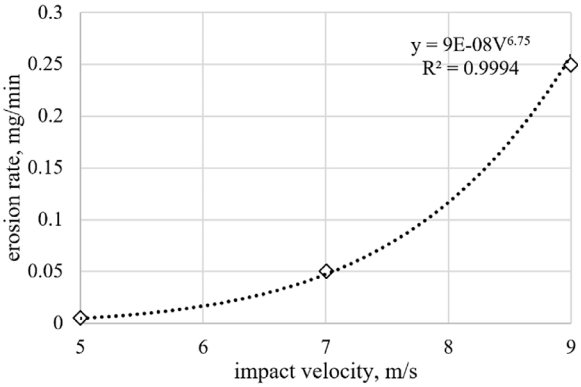


**Figure 4.** The effect of impact velocity on final erosion rate

## Hardness and Hertzian stresses

Solid particle impacts cause the steel surface to undergo intense plastic deformations, which leads to the material hardening by increasing the dislocation density [50]. The change in hardness during erosion tests is an important aspect in testing the erosion resistance of materials. Observations of hardness changes during erosion tests allow us to indicate the limit to which the hardness values increase and after which they stabilize, and thus at what time of exposure such a limit is visible. In the case of an increase in hardness during exposure to erosion damage (Figure 5), it was observed that the increase in hardness at 9 m/s lasted up to 120 min, at 7 m/s up to 240 min, and at 5 m/s until the end of the erosion test, i.e. up to 600 min. Therefore, when testing the same material at different impact velocities, completely different times were obtained at which the hardness values increased. The obtained results were caused by the amount of kinetic energy supplied to the eroded surface of S355J2 steel and the stresses arising in it. As the impact velocity increased, the exposure times associated with the increase in hardness shortened, i.e. not only the time of impact of solid particles on the eroded surface was shortened, but also the stresses in the steel increased, resulting in a greater hardening of the surface layer. A similar relationship was observed during the shot peening process, where an increase in peening pressure and treatment time led to an increase in the final hardness [23]. Skoczylas and Zalewski [51] conducted the shot peening process on gray cast iron EN-GJL 250 and also observed that the increase in impact energy led to the increase in final hardness. Moreover, using balls of smaller diameter resulted in higher final hardness values. The

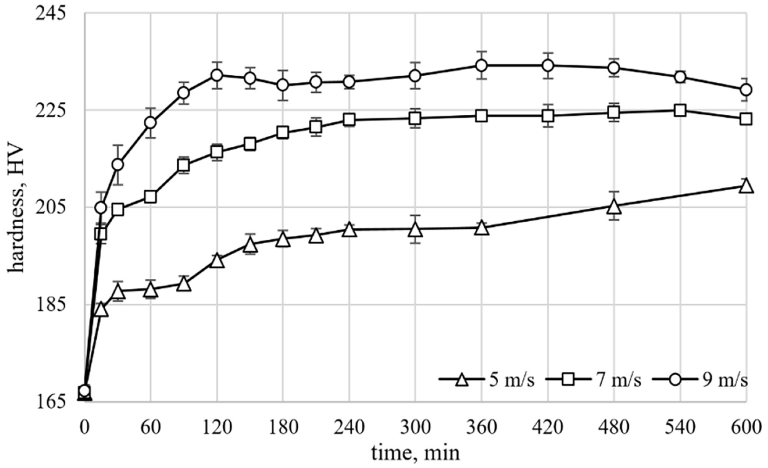


**Figure 5.** Changes in hardness over erosion time

Hertzian stresses are essential to be considered in the studies on solid particle interactions on the steel surface. Under impact, concentrated stresses appear at the point of contact of any particle with the surface. These stresses are a function of material properties, impact velocity, and solid particle (erodent) geometry [52]. Figure 6 schematically shows the pressure distribution when a solid particle hits the eroded surface. Taking into account the Hertz contact theory [40, 53], the mean contact pressure ($P_{mean}$) between the erodent and the sample surface can be calculated and is given by:

$$P_{mean} = \frac{1}{\pi}\left(\frac{5\pi\rho_2}{3}\right)^{1/5}\left(\frac{4S}{3E_1}\right)^{-4/5} V^{2/5} \qquad (2)$$

where: $\rho_2$ is the density of sold particle (erodent), $E_1$ is the Young's Modulus of the target material (S355J2 steel), $V$ is the impact velocity of solid particle, and $S$ is a parameter calculated using the equation below [40,53] (3):

$$S = \frac{9}{16}[(1-\nu_1^2) + ((1-\nu_2^2)(\frac{E_1}{E_2}))] \qquad (3)$$

where: $E_1$ and $v_1$ is the Young's Modulus and Poisson's ratios of the target material (S355J2 steel) and $E_2$ and $v_2$ is the Young's Modulus and Poisson's ratios of the solid particle (cast steel).

Using the above Equation 2, the influence of impact velocity on stress changes in S355J2 steel was presented (Figure 7a). Calculations showed that at the highest impact velocity (9 m/s) mean contact pressure ($P_{mean}$) was approximately 5.5 GPa, while at velocities of 7 m/s and 5 m/s, 4.9 GPa and 4.3 GPa were obtained, respectively. As shown in Figure 7a, the increase in impact velocity led to a linear increase in mean contact pressure in S355J2 steel. The linear increase in Hertzian stress with increasing impact velocity may suggest a proportionality between the kinetic energy of the particles and the stresses generated on the material

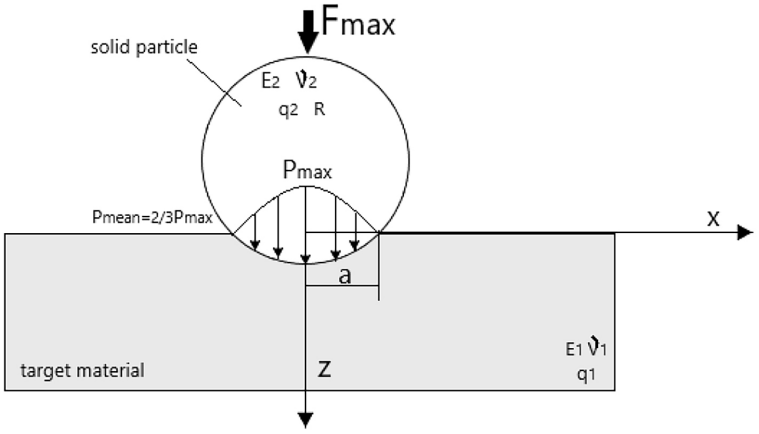


**Figure 6.** Scheme of the Hertz pressure distribution during the impact of a solid particle (erodent) [54]

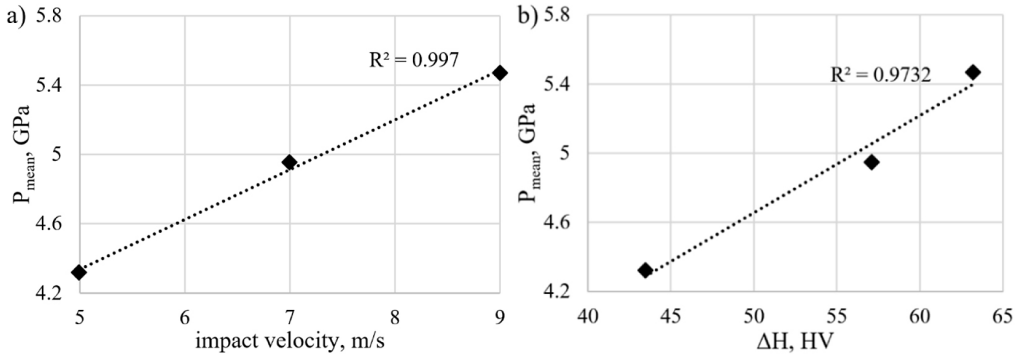


**Figure 7.** Correlation between mean contact pressure and impact velocity (a) and hardness increment ($\Delta H = H_{final} - H_{initial}$) (b)

surface. Therefore, higher kinetic energy of solid particles means higher contact stresses on the surface, which can lead to greater damage, which is in agreement with Johnson [40]. Siepak [55] tested the wear of carburized steel with a high content of retained austenite and found that the increase in contact stress generated greater wear (mass loss), so this is also consistent with the results obtained. The linearity of the increment in Hertzian stresses showed the uniformity of the erosion process for the velocities investigated. This proves that changes in the mechanism of erosion and response of steel to different impact velocities were not sudden, which allows the observation of changes in steel. The eroded steel behaved linearly under changing dynamic conditions. This suggests the cohesion of the material in response to dynamic loads. The predictability over a wide range of erodent impact velocities is important for strength analysis and also design. Moreover, the hardness increment which is the difference between final hardness (after erosion tests) and initial hardness ($\Delta H = H_{final} - H_{initial}$) also showed a linear relationship with the $P_{mean}$ (Figure 7b). During slurry erosion, tested steel was subject to intense deformation, especially in places of contact with solid particles. Increased contact stresses led to plastic deformation of the eroded steel, which affected its hardness. Such relationships (Figure 7) can help predict the erosion resistance of eroded material. Figure 8a shows cross-sections of the steels tested at 5 m/s. The thickness of the deformed layer was 9 ± 1 μm. The energy supplied to the eroded surface was insufficient to cause strong plastic deformations or cracks deep into the material. However, a slight undulation was noticed. The steel grains were slightly flattened. The minor damaged surfaces shown in Figure 8a confirmed very low erosion rates (Figure 3). Cross-sections of the steels tested at 7 m/s are shown in Figure 8b. The thickness of the deformed layer was 14 ± 2 μm. The increase in impact energy resulted in thicker deformed layers. This confirms that the thickness of the deformed layer was an effect of the impact energy. The surface of the S355J2 steel showed undulations and pits with a depth of 1–2 μm (Figure 8b). However, the undulation which is the effect of plastic deformation was higher than in the case of the test performed at a lower impact velocity (5 m/s). The locations marked with white arrows are places of strong deformation, there are voids in their core part. Their shape and location indicate that they were created along deformed grain boundaries. Some cracks (yellow arrows) are also visible in the surface layer, which proves its worse erosion resistance. In the case of the tests performed at 9 m/s, the thickness of the deformed layer was 18 ± 2 μm. Figure 8c confirms strong plastic deformations developed on the eroded surface. Craters resulting from pearlite grain removal are not observed. The most likely reason is their small size (2 μm). Nevertheless, the strong deformation of the uppermost layer and flakes are well visible. In the center of strong deformation (white arrows), voids were formed. Figure 8c indicates that the formation of voids, in particular their development along grain boundaries, was associated with the formation of flakes. Flakes seem to have been the source of the craters. It is believed that cracks develop and gradually spread in weak spots of the steel due to repeated impacts, rather than a single impact. After detachment steel flakes, the strongly deformed area with voids is very vulnerable to subsequent impacts of solid particles. Subsequent impacts probably lead to the removal of material and the formation of craters in highly deformed places.

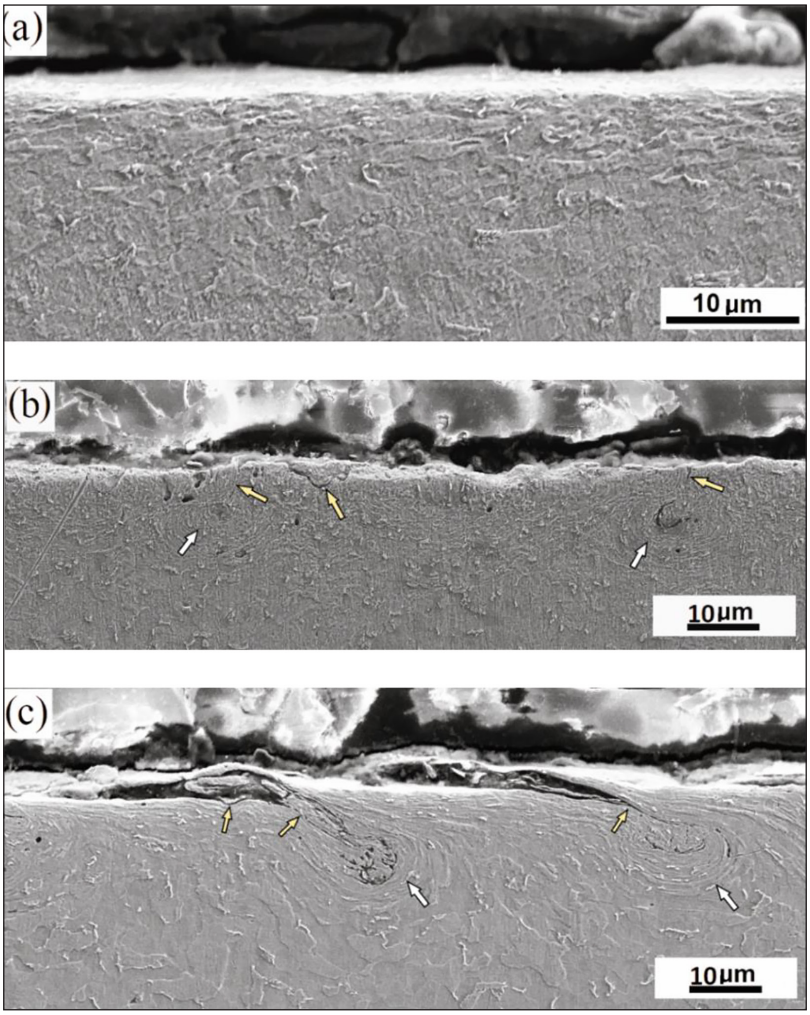


**Figure 8.** Cross sections of S355J2 steel after erosion tests at: (a) 5 m/s, (b) 7 m/s, (c) 9 m/s

The erosion process led to the hardening of the eroded surface due to plastic deformation, which changed the erosion characteristics over time. The lack of strong plastic deformations and cracks at 5 m/s was due to the hardening of the surface layer. As observed (Figure 5), the hardness increased with increasing exposure time, which led to the hardening of the surface layer. However, the kinetic energy of solid particles and mean contact pressure were insufficient to cause serious damage to the eroded surface. The opposite was the case with tests carried out at 7 and 9 m/s, where flaking appeared on the eroded surfaces. The lack of increase in hardness at later exposure times (Figure 5), which was most likely caused by continued depletion of the surface layer by erosion, led to higher erosion rates. Hardening the surface in a short time (Figure 5) leads to the opposite effect, i.e. the material becomes harder but at the same time more brittle and cracks as well as debris occur more easily.

Additionally, the hardness in depth (hardness profiles) of the eroded material was also examined, providing information on the depth of hardening of the surface layer (Figure 9). In this study, the greatest decrease in hardness occurred at a depth of 45 µm, and the hardness at further depths changed slightly for all impact velocities (5, 7, and 9 m/s). Nevertheless, the curves obtained different hardness values in the 0–45 µm section depending on the impact velocity. At a depth of 5 µm, approximately 189 ± 3 HV, 179 ± 2 HV, and 173 ± 2 HV were obtained at 9, 7, and 5 m/s, respectively. However, at a depth of 25 µm, these values decreased by approximately 10, 8 and 6 HV. This indicates that the greatest hardening of the surface layer for all velocities occurred up to 25 µm. The range of hardening depth correlates well with the thickness of the deformed layer (Figure 8). Regardless of the selected target material and test conditions, shot peening produces hardness profiles similar to those obtained

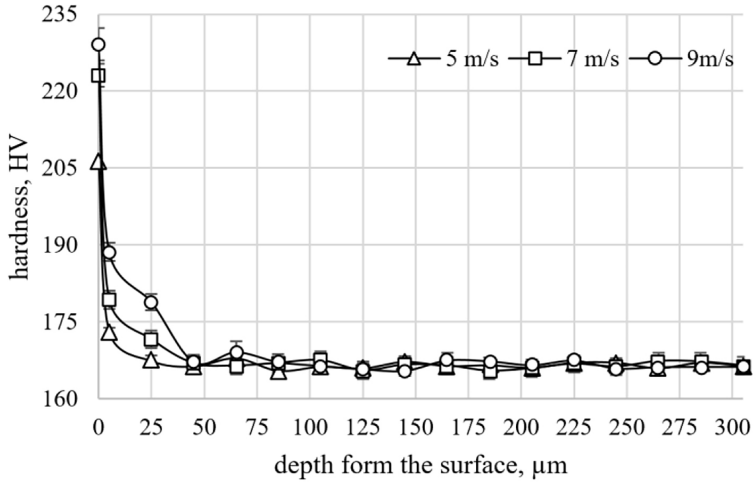


**Figure 9.** Relationship between hardness and distance from the eroded surface (hardness profile)

in slurry erosion [35, 56–59]. The shot peening process causes local hardening of the material surface through strain hardening. Plastic deformations increase the density of dislocations in the crystal structure of the material, which leads to an increase in surface hardness [11].

In the case of erosion tests, the maximum tensile stresses, which were calculated according to Eq. (4), are also important. The impacting solid particle generates maximum tensile stresses on the steel surface in the contact area [60]. Higher tensile stresses lead to greater material damage and therefore lower erosion resistance. At higher impact velocities (7 and 9 m/s), these stresses are clearly higher, which indicates intensification of erosion processes as shown in Figure 10.

$$\sigma_{max} = \frac{1}{2}(1 - 2\nu_1)P_{mean} \qquad (4)$$

Tensile stresses led to surface deformations, which in the long run contributed to the hardening of the surface layer. This was especially visible at the lowest impact velocity (5 m/s), where hardening the surface layer increased resistance to further damage. Nevertheless, at higher velocities, the effect of hardening may be insufficient to compensate for the erosion intensity, which was consistent with the erosion rates obtained (Figure 3a).

Shear stresses calculated according to Hertz's contact theory (Equation 5) provide information about the distribution of stresses in the material near the contact and how deeply these stresses penetrate the tested material. This is crucial for analyzing the strength of the material. The values of maximum shear stresses were directly related to the mechanisms of steel deformation and damage. In general, higher values of maximum shear

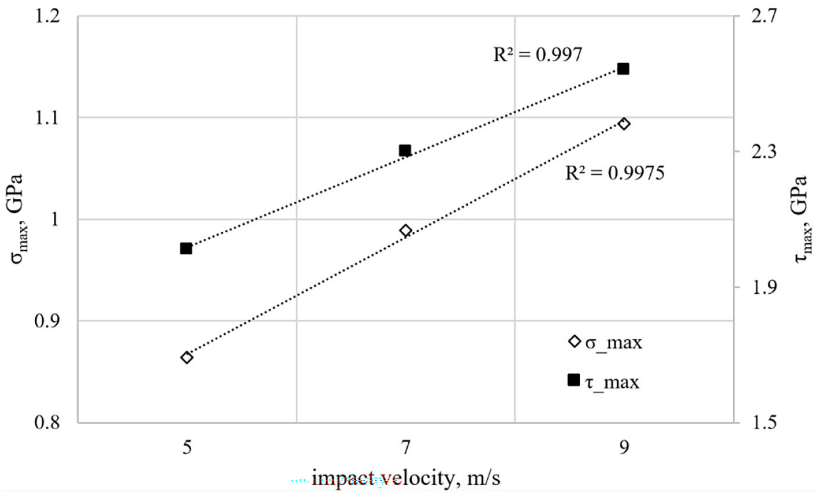


**Figure 10.** Maximum tensile stresses ($\sigma_{max}$) and maximum shear stresses ($\tau_{max}$) as a function of impact velocity

stresses can lead to greater plastic deformations and thus to changes in the hardness of the material (hardening) and even changes in the microstructure of some materials [40].

$$\tau_{max} = 0.31\ (\frac{3P_{mean}}{2}) \tag{5}$$

The analysis of maximum shear stresses (Figure 10) allows the assessment of the influence of various process parameters, such as the impact velocity of solid particles. The effect of the impact velocity on the strength of the material is important in order to optimize working conditions and minimize erosion. Higher maximum shear stresses at higher impact velocities indicate that the eroded steel will be more susceptible to erosion at higher velocities. These stresses lead to greater surface damage and more intensive steel wear. The linear increase in maximum shear stress with impact velocity shows that the effect of velocity on stress is proportional (Figure 10). This increase may suggest that the material has sufficient ductility to partially dissipate impact energy, which may be beneficial in certain applications.

The Hertzian contact theory makes it possible to indicate the depth of maximum shear stresses during the interaction of the tested material – solid particle. This depth is a key place because the material undergoes significant deformation and stress there [40, 61]. The depth of maximum shear stress, *z*, can be calculated as follows:

$$z = 0.48\ a \tag{6}$$

where: $a$ is the mean contact radius (7), and is given by:

$$a = \sqrt{\frac{F_{max}}{\pi P_{mean}}} \tag{7}$$

where: $F_{max}$ is maximum contact load (8) and can be described by:

$$F_{max} = \left(\frac{5\pi\rho_2}{3}\right)^{3/5} (\frac{4S}{3E_1})^{-2/5} R^2 V^{6/5} \tag{8}$$

where: $R$ is the solid particle (erodent) radius.

The depth of maximum shear stresses ($z$) is often similar to the depth at which significant hardening of the material occurs. Therefore, the material hardens most intensely in the places of the highest shear stresses. The efficiency of the hardening can be determined by comparing the material's hardening depth with the depth of maximum shear stress. If the hardening depth is less than the maximum shear stresses depth, this may suggest that the material is not sufficiently resistant to erosion. For impact velocities of 5, 7, and 9 m/s, the calculated maximum shear stress depths (Equation 6) were 11.6, 13.3, and 14.7 μm, respectively. Therefore, the depth of hardening of the surface layer, which reached 0–25 μm, was greater than the depth of maximum shear stresses in this range. The depth of maximum shear stresses is close to the thickness of the deformed layer (Figure 8) and the depth of hardening (Figure 9). In general, shear stresses are only part of the overall stress state in a material. Normal stresses can also play an important role in material deformation. In fact, these stresses can lead to hardening and deformation at greater depths than those predicted by shear stress alone. In the case of velocities of 7 and 9 m/s, as the steel was exposed to repeated impacts (cyclic loads), microcracks and other damage accumulated in it. These damages spread deep into the steel, leading to deformations at a greater depth than would result from a single exposure to maximum shear stresses. However, the higher value of the maximum shear stress than the thickness of the deformed layer, which was formed at velocity of 5 m/s, may indicate that the kinetic energy was not sufficient to create significant plastic deformations in the material, the steel effectively dissipated this amount of impact energy, the supplied energy was mostly contributed to hardening the surface layer. Tillett [62] showed that there is a clear effect of the size of the solid particle on the Hertzian stress. Increasingly higher impact velocities were required to create a crack using smaller solid particles. Therefore, it can be expected that higher impact velocities and an increase in the solid particle size will lead not only to an increase in the erosion rate but also in the stresses in the material. This is consistent with Feng [63] who observed that larger solid particles have high kinetic energy, which leads to increased erosion. This was due to the larger contact surface and contact time in the case of larger erodents.

As observed in Figure 5, hardness changes with the time of exposure to erosion and affects the resistance to further damage. Typically, higher hardness is combined with better erosion resistance [4, 20, 64, 65]. Figure 11 shows the final hardness (after 600 min of testing) as a function of the impact velocity. An increase in impact velocity led to an increase in final hardness. However, it is not related to better erosion resistance. An increase in velocity is also associated with an increase in erosion rate. Therefore, the hardening of the material due to impacting solid particles in the case of S355J2 steel does not have a major impact on the improvement of erosion resistance,

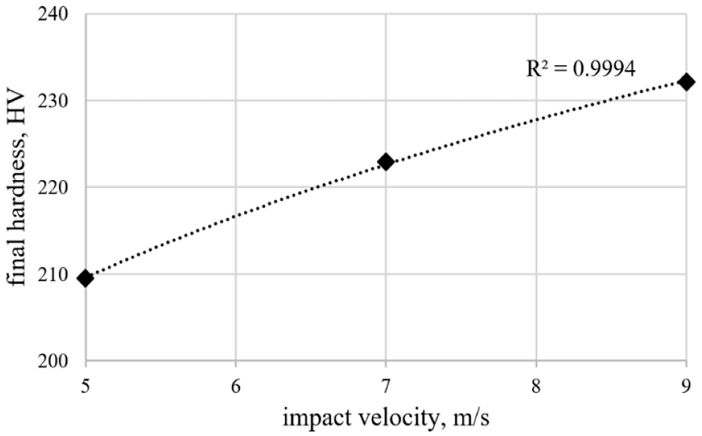


**Figure 11.** Correlation of final hardness (after erosion tests) and impact velocity

but leads to easier and faster formation of cracks on the steel surface and their propagation into the material, which is consistent with the results of the erosion rate.

## Damage characterization after slurry erosion tests

The microscopic examinations of S355J2 ferritic-pearlitic steel after the slurry tests are presented in Figure 12. Mechanisms of slurry erosion are intricate. Slurry erosion mechanisms are significantly influenced by impact velocity. Depending on the operating conditions, the size, shape, and trajectory of the erodent particle, many mechanisms were discovered acting simultaneously. Erosion tests carried out on the S355J2 steel at the impact velocity of 5 m/s (Figure 12a and 12b) showed undulations due to plastic deformation as well as craters and pits with a diameter of 2–8 μm. The applied stresses did not lead to the formation of cracks on the eroded surface or steel flakes, which was related to the gradual hardening of the surface layer (Figure 5). In the case of the impact velocity of 7 m/s (Figure 12c and 12d), steel flakes, microcracks and indentations appeared. The indentations were small, having a diameter of 1 μm to 5 μm. Increasing the impact velocity by 2 m/s contributed to the formation of small steel flakes, their deformation and the appearance of debris. With the increase of the impact velocity to 9 m/s (Figure 12e and 12f), more and extensive steel flakes, microcracks and cracks as well as debris appeared on the eroded surface. The indentations and pits became shallower and their diameter ranged from 1 μm to 3 μm. In the case of an impact velocity of 9 m/s, the erosion damage to S355J2 steel was more serious, resulting from large steel flakes detaching from the eroded surface. It resulted in more severe wear.

During contact between the solid particle and the eroded material, the deformed material was extrusion of the contact zone. Thus subsequent impacts of solid particles, the resulting steel flakes fragment (7 and 9 m/s). Considering the impact velocity 7 and 9 m/s, it looks as if the formation of flakes were the source which could significantly reduce the strength of S355J2 steel. Furthermore, solid particles hitting the eroded steel surface cause local stresses that are cyclically repeated with each impact. As in the case of impact velocities of 7 and 9 m/s, these stresses led to microcracks, which over time can propagate into the steel, causing material fatigue. Moreover, any surface defect may become a source of fatigue cracks, which will develop under the influence of further cyclic loads. Over time, surface damage accumulates. Even minor damage can lead to more serious fatigue problems over time because stress is concentrated at the defects, which accelerates the development of cracks. At higher impact velocities, in addition to the fatigue mechanism, there was also a platelet mechanism of erosion associated with the appearance of steel flakes on the eroded surfaces. During the interaction between the solid particle and the surface of the target material, the deformed material is squeezed out of the contact zone. Continued impacts of solid particles cause fracture of the formed steel flakes as shown in Figure 12d and 12f as well as then their cracking and detachment from the eroded surface like in [17, 66].

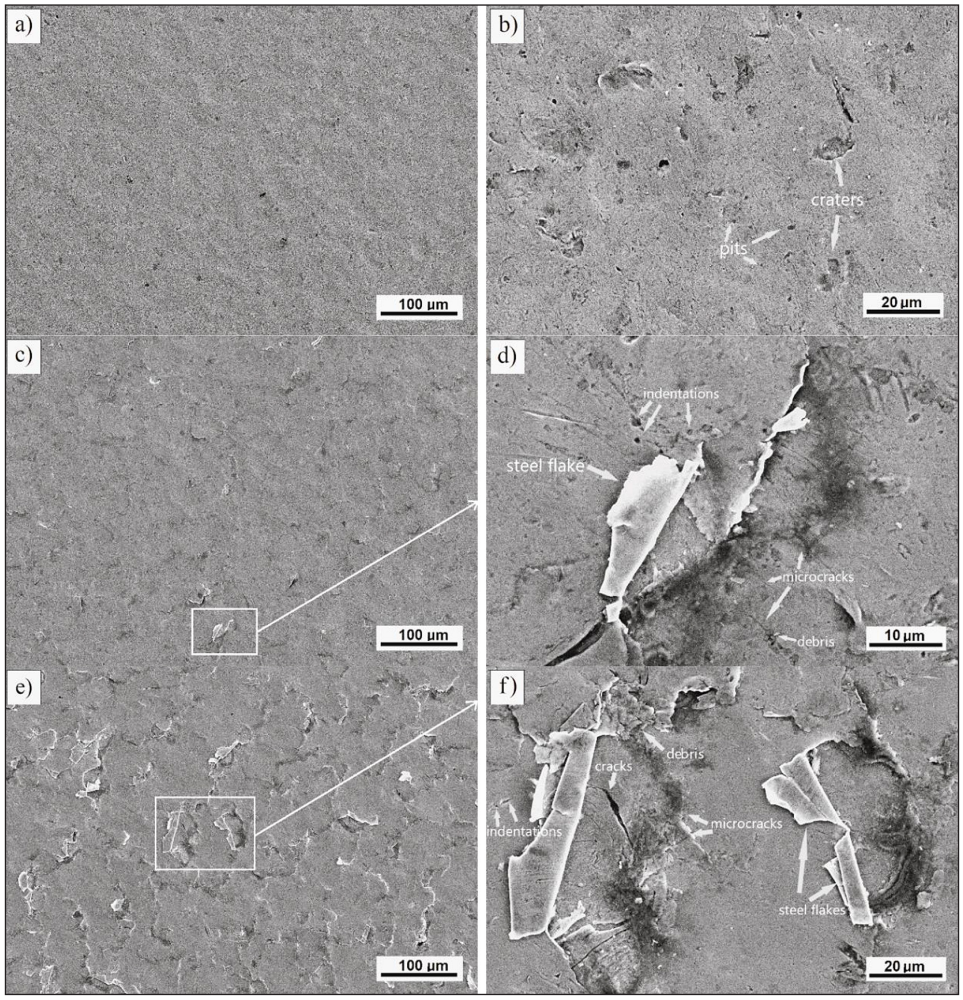


**Figure 12.** SEM images after the erosion tests at impact velocity 5 m/s (a, b), 7 m/s (c, d) and 9 m/s (e, f)

Taking into account the obtained results of erosion tests, a scheme of erosion mechanisms in the tested S355J2 steel can be presented (Figure 13). The collected research results show a certain pattern. Analyzing the SEM images of the eroded surface (Figure 12) and cross-sections (Figure 8), it was observed that increasing the impact velocity and thus the kinetic energy supplied to the tested steel leads to the formation of similar deformations of the eroded surfaces. As mentioned above, tests carried out at an impact velocity of 5 m/s showed that the steel surface did not have significant surface deformations, mainly craters and pits. Therefore, the surface layer is hardened first without any visible spalling (steel flakes), only the surface is hardened, protecting the steel against excessive erosion rates (I). In the second stage (II), as the exposure time increases, the first stronger deformations appear (surface hardness stabilizes), then the first microcracks and small steel flakes

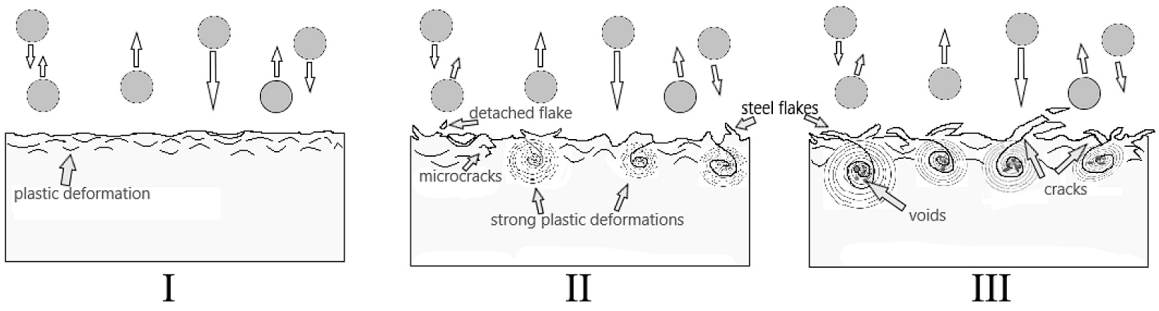


**Figure 13.** Scheme of impact of rebounding solid particles on the degradation process of S355J2 steel

appear. The plastically deformed steel flakes are subsequently removed upon further impact from solid particles. In the third stage (III), large plastic deformations appear, strongly deformed and large steel flakes, cracks are more visible, and voids may become a source of cracks and craters. Subsequent impacts with solid particles lead to detachment of steel flakes and material fatigue.

## CONCLUSIONS

In the present study, the influence of impact velocity on Hertzian stresses and failure of S355J2 steel was investigated. The slurry erosion resistance of S355J2 was tested at impact velocity of 5, 7, and 9 m/s. The following conclusions are derived from the presented slurry erosion tests:

- A significant increase in erosion rate was observed at 9 m/s. This increase was fivefold and over fiftyfold compared to the velocity of 7 and 5 m/s, respectively. Under test conditions, S355J2 steel was characterized by a velocity exponent $n$ of 6.75.
- A linear relationship between the mean contact pressure and the impact velocity and hardness increase ($\Delta H$) was observed. This proves that the erosion process is uniform in the tested range of impact velocities.
- The hardness profile indicates significant work hardening. The surface layer behaves similarly to the shot peening process. As the slurry erosion intensity increase, the depth of work hardening layer increase. Moreover, the range of hardening depth correlates well with the thickness of the deformed layer.
- The linear increase in maximum shear stress with impact velocity indicates that the effect of velocity on stress is proportional. This suggests that the material has enough ductility to partially dissipate impact energy.
- The depth at which maximum shear stresses occur is often similar to the depth at which significant hardening of the material takes place. The depth of maximum shear stresses was close to the thickness of the deformed layer and the depth of hardening.
- The dominant type of deformation mechanism was fatigue degradation of the surface layers of the eroded steels. The increase in impact velocity and Hertzian stresses led to an increase in the number of flakes on the eroded surface after erosion tests.

## Acknowledgements

The authors would like to thank Alicja Krella, Prof., D.Sc., Ph.D., Eng. for her support and for providing the measurement stand as well as laboratory equipment.

## REFERENCES

1. Javaheri V., Porter D., Kuokkala V.T. Slurry erosion of steel – Review of tests, mechanisms and materials. Wear 2018; 408–409: 248–73. https://doi.org/10.1016/j.wear.2018.05.010
2. Clark H.M. The influence of the flow field in slurry erosion. Wear 1992, 152:223–40. https://doi.org/10.1016/0043-1648(92)90122-O
3. Grewal H.S., Agrawal A., Singh H. Design and development of high-velocity slurry erosion test rig using CFD. Journal of Materials Engineering and Performance 2013; 22: 152–61. https://doi.org/10.1007/s11665-012-0219-y
4. Ojala N., Valtonen K., Antikainen A., Kemppainen A., Minkkinen J., Oja O. Wear performance of quenched wear resistant steels in abrasive slurry erosion. Wear 2016; 354–355: 21–31. https://doi.org/10.1016/j.wear.2016.02.019
5. Buszko M.H., Krella A.K., Marchewicz A., Gajowiec G. Effect of annealing temperature on slurry erosion resistance of ferritic X10CrAlSi18 steel. Tribology International 2021; 153: 106648. https://doi.org/10.1016/j.triboint.2020.106648
6. Krella A.K., Buszko M.H., Gajowiec G. Degradation of ferritic X10CrAlSi18 stainless steel caused by slurry. Engineering Failure Analysis 2020; 116: 104696. https://doi.org/10.1016/j.engfailanal.2020.104696
7. Buszko M.H., Krella A.K. An influence of factors of flow condition, particle and material properties on slurry erosion resistance. Advances in Materials Science 2019; 19: 28–53. https://doi.org/10.2478/adms-2019-0010
8. Buszko M.H., Krella A.K. Slurry erosion – Design of test devices. Advances in Materials Science 2017; 17: 5–17. https://doi.org/10.1515/adms-2017-0007
9. Skoczylas A. The effect of vibratory shot peening on the geometric structure of the surface of elements machined by laser and abrasive water jet cutting. Advances in Science and Technology Research Journal 2023; 17: b1–11. https://doi.org/10.12913/22998624/170970
10. Bławucki S., Zaleski K. The numerical FEM Model of the kinematics of the vibratory shot peening process. Advances in Science and Technology Research Journal 2017; 11: 260–9. https://doi.

org/10.12913/22998624/80841

11. Świetlicki A., Szala M., Walczak M. Effects of shot peening and cavitation peening on properties of surface layer of metallic materials—A short review. Materials 2022; 15. https://doi.org/10.3390/ma15072476
12. Oka Y.I., Okamura K., Yoshida T. Practical estimation of erosion damage caused by solid particle impact: Part 1: Effects of impact parameters on a predictive equation. Wear 2005; 259: 95–101. https://doi.org/10.1016/j.wear.2005.01.039
13. Patil M.S., Deore E.R., Jahagirdar R.S., Patil S.V. Study of the parameters affecting erosion wear of ductile material in solid-liquid mixture. World Congress on Engineering 2011; III.
14. Nguyen Q.B., Lim C.Y.H., Nguyen V.B., Wan Y.M., Nai B., Zhang Y.W. Slurry erosion characteristics and erosion mechanisms of stainless steel. Tribology International 2014; 79: 1–7. https://doi.org/10.1016/j.triboint.2014.05.014
15. Desale G.R., Gandhi B.K., Jain S.C. Slurry erosion of ductile materials under normal impact condition. Wear 2008; 264: 322–30. https://doi.org/10.1016/j.wear.2007.03.022
16. López D., Congote J.P., Cano J.R., Toro A., Tschiptschin A.P. Effect of particle velocity and impact angle on the corrosion-erosion of AISI 304 and AISI 420 stainless steels. Wear 2005; 259: 118–24. https://doi.org/10.1016/j.wear.2005.02.032
17. Alam T., Islam M.A., Farhat Z.N. Slurry erosion of pipeline steel: effect of velocity and microstructure. Journal of Tribology 2016; 138: 1–10. https://doi.org/10.1115/1.4031599
18. Akbarzadeh E., Elsaadawy E., Sherik A.M., Spelt J.K., Papini M. The solid particle erosion of 12 metals using magnetite erodent. Wear 2012; 282–283: 40–51. https://doi.org/10.1016/j.wear.2012.01.021
19. Mbabazi J.G., Sheer T.J., Shandu R. A model to predict erosion on mild steel surfaces impacted by boiler fly ash particles. Wear 2004; 257: 612–24. https://doi.org/10.1016/j.wear.2004.03.007
20. Alam T., Farhat Z.N. Slurry erosion surface damage under normal impact for pipeline steels. Engineering Failure Analysis 2018; 90: 116–28. https://doi.org/10.1016/j.engfailanal.2018.03.019
21. Shitole P.P., Gawande S.H., Desale G.R., Nandre B.D. Effect of Impacting Particle Kinetic Energy on Slurry Erosion Wear. Journal of Bio- and Tribo-Corrosion 2015; 1: 1–9. https://doi.org/10.1007/s40735-015-0028-6
22. Malik J., Toor I.H., Ahmed W.H., Gasem Z.M., Habib M.A., Ben-Mansour R. Evaluating the effect of hardness on erosion characteristics of aluminum and steels. Journal of Materials Engineering and Performance 2014; 23: 2274–82. https://doi.org/10.1007/s11665-014-1004-x
23. Walczak M., Matijošius J., Özkan D., Pasierbiewicz K. Effect of shot peening parameters on surface properties and corrosion resistance of 316L stainless steel. Advances in Science and Technology Research Journal 2024; 18: 296–304. https://doi.org/10.12913/22998624/186513
24. Singh J., Vasudev H., Szala M., Gill H.S. Neural computing for erosion assessment in Al-20TiO2 HVOF thermal spray coating. International Journal on Interactive Design and Manufacturing 2024; 18: 2321–32. https://doi.org/10.1007/s12008-023-01372-y
25. Desale G.R., Gandhi B.K., Jain S.C. Particle size effects on the slurry erosion of aluminium alloy (AA 6063). Wear 2009; 266: 1066–71. https://doi.org/10.1016/j.wear.2009.01.002
26. Lathabai S. Effect of grain size on the slurry erosive wear of Ce-TZP ceramics. Scripta Materialia 2000; 43: 465–70. https://doi.org/10.1016/S1359-6462(00)00415-2
27. Clark H.M., Hartwich R.B. A re-examination of the "particle size effect" in slurry erosion. Wear 2001; 248: 147–61. https://doi.org/10.1016/S0043-1648(00)00556-1
28. Lindgren M., Perolainen J. Slurry pot investigation of the influence of erodent characteristics on the erosion resistance of austenitic and duplex stainless steel grades. Wear 2014; 319: 38–48. https://doi.org/10.1016/j.wear.2014.07.006
29. Desale G.R., Gandhi B.K., Jain S.C. Effect of erodent properties on erosion wear of ductile type materials. Wear 2006; 261: 914–21. https://doi.org/10.1016/j.wear.2006.01.035
30. Desale G.R., Gandhi B.K., Jain S.C. Effect of physical properties of solid particle on erosion wear of ductile materials. World Tribology Congress III, 1, ASME 2005; 149–50. https://doi.org/10.1115/WTC2005-63997
31. Vite-Torres M., Laguna-Camacho J.R., Baldenebro-Castillo R.E., Gallardo-Hernández E.A., Lasorsa C.A., Villagrán-Villegas L.Y. Study of solid particle erosion on AISI D2 using angular silicon carbide and steel round grit particles. Tribology - Materials, Surfaces and Interfaces 2014; 8: 105–10. https://doi.org/10.1179/1751584X13Y.0000000057
32. Vite-Torres M., Laguna-Camacho J.R., Baldenebro-Castillo R.E., Gallardo-Hernández EA, Vera-Cárdenas E.E., Vite-Torres J. Study of solid particle erosion on AISI 420 stainless steel using angular silicon carbide and steel round grit particles. Wear 2013; 301: 383–9. https://doi.org/10.1016/j.wear.2013.01.071
33. Babu P.S., Basu B., Sundararajan G. The influence of erodent hardness on the erosion behavior of detonation sprayed WC-12Co coatings. Wear 2011; 270: 903–13. https://doi.org/10.1016/j.wear.2011.02.019

34. Ojala N., Valtonen K., Kivikytö-Reponen P., Vuorinen P., Kuokkala V.T. High speed slurry-pot erosion wear testing with large abrasive particles. TRIBOLOGIA - Finnish Journal of Tribology 2015; 33: 36–44.
35. Świetlicki A., Walczak M., Szala M. Effect of shot peening on corrosion resistance of additive manufactured 17-4PH steel. Materials Science-Poland 2022; 40: 135–51. https://doi.org/10.2478/msp-2022-0038
36. Nguyen Q.B., Nguyen V.B., Lim C.Y.H., Trinh Q.T., Sankaranarayanan S., Zhang Y.W. Effect of impact angle and testing time on erosion of stainless steel at higher velocities. Wear 2014; 321: 87–93. https://doi.org/10.1016/j.wear.2014.10.010
37. Kübarsepp J., Juhani K., Tarraste M. Abrasion and erosion resistance of cermets: A review. Materials 2022; 15. https://doi.org/10.3390/ma15010069
38. Hussainova I., Kubarsepp J., Pirso J. Mechanical properties and features of erosion of cermets. Wear 2001; 250–251: 818–25. https://doi.org/10.1016/S0043-1648(01)00737-2
39. Barber J., Mellor B.G., Wood R.J.K. The development of sub-surface damage during high energy solid particle erosion of a thermally sprayed WC-Co-Cr coating. Wear 2005; 259: 125–34. https://doi.org/10.1016/j.wear.2005.02.008
40. Johnson K.L. Contact mechanics. Cambridge University Press, 1985.
41. Kirchner H.P., Gruver R.M. Localized impact damage in glass. Materials Science and Engineering 1977; 28: 153–60. https://doi.org/10.1016/0025-5416(77)90099-4
42. Ojala N., Valtonen K., Minkkinen J., Kuokkala V.T. Edge and particle embedment effects in low- and high-stress slurry erosion wear of steels and elastomers. Wear 2017; 388–389: 126–35. https://doi.org/10.1016/j.wear.2017.06.004
43. Ojala N., Valtonen K., Heino V., Kallio M., Aaltonen J., Siitonen P. Effects of composition and microstructure on the abrasive wear performance of quenched wear resistant steels. Wear 2014; 317: 225–32. https://doi.org/10.1016/j.wear.2014.06.003
44. Katsumata T., Matsubara T., Yamamoto K., Iwai Y. Evaluation of coating properties with a Micro Slurry-jet Erosion (MSE) test: – Effects of the shape and size of erodent particles on erosion behaviors of TiN coating –. Surface and Coatings Technology 2021; 421: 127443. https://doi.org/10.1016/j.surfcoat.2021.127443
45. Liang L., Pang Y., Tang Y., Zhang H., Liu H., Liu Y. Combined wear of slurry erosion, cavitation erosion, and corrosion on the simulated ship surface. Advances in Mechanical Engineering 2019; 11: 1–14. https://doi.org/10.1177/1687814019834450
46. Borko K., Hadzima B., Pastorek F. The corrosion properties of S355J2 steel welded joint in chlorides environment. Periodica Polytechnica Transportation Engineering 2018; 1–6. https://doi.org/10.3311/PPtr.12111
47. Miarka P., Cruces A.S., Seitl S., Malíková L., Lopez-Crespo P. Influence of the constraint effect on the fatigue crack growth rate in S355 J2 steel using digital image correlation. Fatigue and Fracture of Engineering Materials and Structures 2020; 43: 1703–18. https://doi.org/10.1111/ffe.13198
48. Sapate S.G., RamaRao A.V. Effect of erodent particle hardness on velocity exponent in erosion of steels and cast irons. Materials and Manufacturing Processes 2003; 18: 783–802. https://doi.org/10.1081/AMP-120024975
49. Duan C.G., Karelin V.Y. Abrasive erosion and corrosion of hydraulic machinery, 2002; 2. https://doi.org/10.1142/9781848160026
50. Singh J., Nath S.K. Microstructural characterization and investigation of slurry erosion performance of cyclically heat treated martensite steel. Engineering Failure Analysis 2022; 131: 105833. https://doi.org/10.1016/j.engfailanal.2021.105833
51. Skoczylas A., Zaleski K. Effect of regular shot peening and semi-random shot peening conditions on selected properties of the surface layer of gray cast iron. Advances in Science and Technology Research Journal 2024; 18: 284–95. https://doi.org/10.12913/22998624/184341
52. Sheldon G.L., Finnie I. The mechanism of material removal in the erosive cutting of brittle materials. Journal of Manufacturing Science and Engineering, Transactions of the ASME 1966; 88: 393–9. https://doi.org/10.1115/1.3672667
53. Wheeler D.W., Wood R.J.K. Solid particle erosion behaviour of CVD boron phosphide coatings. Surface and Coatings Technology 2006; 200: 4456–61. https://doi.org/10.1016/j.surfcoat.2005.03.011
54. Shaw L.L. The surface deformation and mechanical behavior of nanostructured alloys. Woodhead Publishing Limited, 2011. https://doi.org/10.1533/9780857091123.3.481
55. Siepak J. The influence of contact stress on the wear of a carburized steel case with a high content of retained austenite. Wear 1982, 80: 301–5. https://doi.org/10.1016/0043-1648(82)90258-7
56. Maleki E., Unal O., Reza Kashyzadeh K., Bagherifard S., Guagliano M. A systematic study on the effects of shot peening on a mild carbon steel: Microstructure, mechanical properties, and axial fatigue strength of smooth and notched specimens. Applied Surface Science Advances 2021; 4. https://doi.org/10.1016/j.apsadv.2021.100071
57. Nordin E, Alfredsson B. Experimental investigation of shot peening on case hardened SS2506 gear steel.

Experimental Techniques 2017; 41: 433–51. https://doi.org/10.1007/s40799-017-0183-4

58. Tekkalmaz M., Er Ü., Çakir F.H., Bozkurt F. A new approach to monitoring the operational success of shot peening with electromechanical impedance technique. International Journal of Advanced Manufacturing Technology 2021; 117: 3503–13. https://doi.org/10.1007/s00170-021-07933-3
59. Wu D., Yao C., Zhang D. Surface characterization of Ti1023 alloy shot peened by cast steel and ceramic shot. Advances in Mechanical Engineering 2017; 9: 1–14. https://doi.org/10.1177/1687814017723287
60. Lu J.-W., Sargent G.A., Conrad H. A study of the fundamental mechanisms of erosion using Hertzian fracture tests. Wear 1993; 162–164: 856–63. https://doi.org/10.1016/0043-1648(93)90087-3
61. Wheeler D.W., Wood R.J.K. The fracture of diamond coatings by high velocity sand erosion. Philosophical Magazine 2009; 89: 285–310.
62. Tillett J.P.A. Fracture of glass by spherical indenters. Proceedings of the Physical Society Section B 1956; 69: 47–54. https://doi.org/10.1088/0370-1301/69/1/306
63. Feng Z. The Erosion of Materials. Cape Town, 1998.
64. Jonda E., Łatka L., Lont A., Gołombek K., Szala M. The effect of HVOF spray distance on solid particle erosion resistance of WC-based cermets bonded by Co, Co-Cr and Ni deposited on Mg-alloy substrate. Advances in Science and Technology Research Journal 2024; 18: 115–28. https://doi.org/10.12913/22998624/184025
65. Majewski D., Hejwowski T., Łukasik D. The influence of microstructure of arc sprayed coatings on wear resistance. Advances in Science and Technology Research Journal 2018; 12: 285–92. https://doi.org/10.12913/22998624/86210
66. Grewal H.S., Agrawal A., Singh H. Slurry erosion mechanism of hydroturbine steel: Effect of operating parameters. Tribology Letters 2013; 52: 287–303. https://doi.org/10.1007/s11249-013-0213-z